

Edge-driven rotating magnetic field current drive of field-reversed configurations

Richard D. Milroy and Kenneth E. Miller

University of Washington, Redmond Plasma Physics Laboratory, 14700 NE 95th Street, Redmond, Washington 98052

(Received 19 September 2003; accepted 20 November 2003)

Field-reversed configurations (FRCs) are created and sustained using a rotating magnetic field (RMF) in the Translation Confinement and Sustainment experiment. Normally this experiment is operated in a manner where the RMF only partially penetrates the plasma column. This method of operation may have significant advantages in producing less disturbances to the bulk of the FRC, but requires driving an overall radially inward flow to maintain $E_\theta(r) = 0$ everywhere (through the $V_r B_z$ term in the generalized Ohm's law). However, some RMF penetration is still required at the field null R , where $B_z = 0$. For some experimental conditions it appears that the RMF does not even penetrate as far as the null, raising the question as to how $E_\theta(r=R)$ can be maintained at zero despite a finite $\eta_\perp j_\theta(r=R)$. Numerical simulations with a resistivity profile that is sharply peaked near the plasma edge yield similar profiles, and provide insight into this physical process. An inner magnetic structure forms, which rotates at a much lower frequency than the RMF. A tearing and reconnection process produces a torque transfer from the outer RMF to the inner structure, allowing it to act as an RMF downshifted to a lower frequency, and thus provide current drive to the inner region of the FRC. This mode of RMF current drive is being called "edge-driven mode." © 2004 American Institute of Physics. [DOI: 10.1063/1.1641381]

I. INTRODUCTION

A transverse rotating magnetic field (RMF) can be used to drive toroidal current in a compact toroid (CT). RMF current drive was first investigated by Blevin and Thonemann¹ in the 1950s and then studied extensively at Flinders University in a device called the Rotamak.² At the University of Washington (RPPL), the Translation, Confinement and Sustainment^{3,4} (TCS) experiment was built to study RMF current drive in field-reversed configurations (FRCs). In both this device and the previous Star Thrust Experiment⁵ (STX), FRCs have been successfully formed and sustained through the application of the RMF to background gas immersed in a forward bias field.

An internal magnetic probe has been used to measure the magnetic field profile in the TCS experiment over a wide range of parameters, including antenna length and RMF frequency. Normally, both this and the STX experiment were operated in a mode where the RMF did not penetrate to the axis of symmetry, but to a point near the magnetic null. Good agreement has been reported between numerical simulations using a two-dimensional (2D) ($r-\theta$) code,⁶ and the experimental measurements. Both the code and experiments showed a characteristic flattening of the radial axial magnetic field profile $B_z(r)$ near the magnetic field null, and a radial RMF profile where the RMF penetrated slightly beyond the null. However, it has been found recently that for some experimental conditions in TCS, equilibrium was reached where the RMF did not even penetrate to the null, and there was no distinctive flattening in the $B_z(r)$ profile. For these experimental conditions, our previous explanation⁶ for the physics of partial penetration, namely that a radial flow u_r ,

forms such that the $u_r \times B_z$ component of Ohm's law generates the needed azimuthal electric field E_θ on the inner field lines, is inadequate. The calculations demand that the RMF penetrate at least to the magnetic null since $B_z = 0$ there. It was found that if a resistivity profile that is sharply peaked near the wall is assumed in the RMF code, results similar to the recent experimental observations were obtained. The predicted B_z profiles no longer had a distinct flattening near the null, in agreement with the experimental data. A resistivity profile that is peaked near the wall could be produced by micro-instabilities due to the large electron velocities induced by the RMF at large radius, or due to other effects introduced by the RMF itself.⁷

If the ions are not rotating azimuthally, and all of the electrons are rotating synchronously with the RMF, the azimuthal line current is $I'_{\text{sync}} = 0.5 \langle n_e \rangle e r_s^2 \omega_{\text{RMF}}$, where ω_{RMF} is the rotation rate of the RMF, r_s is the separatrix radius, and $\langle n_e \rangle$ is the average electron density, so that the electron line density is $\pi \langle n_e \rangle r_s^2$. From Faraday's law, the actual azimuthal line current is $I'_{\text{rev}} = (B_{z\text{Ext}} - B_{z0}) / \mu_0$, where $B_{z\text{Ext}}$ is the axial magnetic field external to the FRC, and B_{z0} is the axial magnetic field at the axis of symmetry. The ratio of these two azimuthal line currents is $\zeta = I'_{\text{rev}} / I'_{\text{sync}} \approx 4 B_{z\text{Ext}} / \mu_0 \langle n_e \rangle e \omega_{\text{RMF}} r_s^2$. Here B_{z0} is approximated as $-B_{z\text{Ext}}$, so $(B_{z\text{Ext}} - B_{z0}) \approx 2 B_{z\text{Ext}}$. ζ is an important parameter for characterizing RMF current drive. When it is small, most electrons are not rotating synchronously with the RMF, and consequently the RMF cannot penetrate deeply into the FRC. Conversely, when ζ approaches one, most of the electrons are rotating synchronously with the RMF, and the RMF penetrates deeply into the FRC. The phenomenon described

in this paper was most prominent in low ζ shots.

This paper will present a description of the new physical process resulting from a non-uniform resistivity profile, and compare experimental data with numerical predictions. Section II provides a description of the experimental measurements, the RMF code, and the previously assumed physical mechanism for partial RMF penetration. In Sec. III, numerical calculations will be compared with experimental data as evidence that a newly discovered physical mechanism can transfer torque applied to the electrons in the outer region where the primary RMF field penetrates, inward to the electrons at the magnetic field null and beyond. A discussion and conclusions are presented in Sec. IV.

II. BACKGROUND

A. Internal magnetic probe

The internal magnetic field was measured on TCS using a 420 mm long by 6 mm diameter probe containing 31 magnetic pickup loops. The probe was inserted at the axial mid-plane of the FRC and extended from the wall to the axis of symmetry. The first 11 loops were spaced 20 mm apart and spanned from $r=0$ to $r=200$ mm. The remaining 20 loops were spaced 10 mm apart and spanned from $r=210$ to $r=400$ mm, providing higher spatial resolution in the outer region where the magnetic field gradients were larger. Each loop was wound on a 9 mm long by 1 mm wide frame and consists of 30 turns of 37 μm diameter gold plated tungsten wire.

The probe could be rotated so that the loops aligned to measure only the axial magnetic field B_z , or only the transverse magnetic field B_θ . Normally the probe was rotated half-way between the B_z and B_θ extremes with the recorded signals containing some of both. The θ -component was then assumed to be from the RMF and thus oscillate at the RMF frequency f_{RMF} . Therefore, the signal within ± 10 kHz of the RMF frequency was defined to be in the θ -direction, and the rest of the signal was defined to be in the z direction. The validity of these assumptions was tested by firing a sequence of identical shots with the probe in each of the three positions. For most analysis these assumptions could be safely used, although there were certain instances where they could not be.

Two addition points are worth mentioning. The first is that although B_θ implies the azimuthal component of the magnetic field in cylindrical coordinates (assuming cylindrical symmetry of the various modes, and the RMF being a pure $n=1$ mode), the probe really measured just the transverse field along one radial cord. The second is that when B_θ is plotted versus radius at a given time (as it is in several of the figures) it is really the magnitude of the envelope of the B_θ signal that is plotted. This is done to show the characteristic RMF amplitude of the oscillatory B_θ signal versus radius.

B. RMF code

Numerical simulations have been made using a 2D magnetohydrodynamic (MHD) ($r-\theta$) code that has been de-

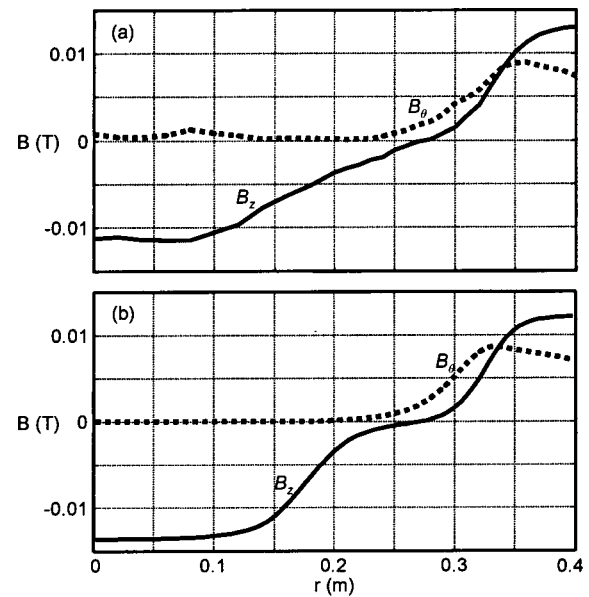


FIG. 1. Experimental (a) and numerically calculated (b) magnetic field profiles for an RMF driven FRC.

scribed previously.⁶ It is important to note that while this model advances the MHD equations in the ($r-\theta$) plane, the equations have been modified to include some three dimensional (3D) effects that are essential for RMF current drive. The equations are modified to account for an axial equilibrium based on $\langle\beta\rangle = 1 - \frac{1}{2}x_s^2$, where x_s is the FRC's separatrix radius divided by the external axial flux conserver's radius. Also, flow parallel to the magnetic field lines tends to equalize pressure between the connected inner and outer field lines. The model includes terms that make this pressure adjustment. In Ref. 6, pressure was equalized between connected inner and outer field lines assuming no rotation. In the present version of the code, the ions are allowed to rotate and the effects of centripetal force are correctly accounted for. In this case the pressure between connected inner and outer field lines at radii r_i and r_o can be expressed as

$$\frac{P_o}{P_i} = \exp\left\{\frac{m_i\omega^2}{2kT_{\text{ave}}}(r_o^2 - r_i^2)\right\},$$

where P_o is the pressure on the outer field lines, P_i is the pressure on the corresponding inner field line, m_i is the ion mass, ω is the rotation velocity, and T_{ave} is the average temperature on the field line.

In most previous simulations, a constant and uniform plasma resistivity was assumed. In this paper we explore the effects of using a resistivity that is peaked near the vacuum vessel wall.

C. Partial penetration

For most of the experimental data produced by the TCS experiment, the RMF only penetrated the outer region of the FRC, reaching in to a point just slightly past the magnetic field null. A typical TCS magnetic field profile is illustrated in Fig. 1(a). This profile can be compared with that of a numerical simulation with uniform resistivity (150 $\mu\Omega\text{m}$)



FIG. 2. RMF field lines inferred from experimental data.

and similar parameters, shown in Fig. 1(b). The overall agreement is reasonably good. The B_θ profile is observed to increase with distance from the wall, and then decrease to a small value inside of the magnetic null. The B_z profile decreases sharply with distance from the wall and flattens somewhat near the null. The biggest difference between the experimental and the numerical profiles is the degree of flattening near the null. Previously experimental profiles showing distinct flattening near the null have been reported for both STX⁸ and TCS,⁴ but the profile shown in Fig. 1(a) is more typical of recent TCS operation.

The shape of the RMF field lines, as inferred from the probe data is shown in Fig. 2. As the RMF rotates in a counter-clockwise direction, it exerts a torque on the electrons. Due to resistivity, the electrons rotate slightly slower than the RMF and tend to pull the field lines back in the opposite direction. This leads to RMF screening currents as well as RMF phase slippage, as can be seen by the bending and wrapping of the field lines shown in Fig. 2.

The RMF applies a torque to the electrons in the outer region where it has penetrated. However, current drive must also be applied to the inner region of the FRC where the RMF has not penetrated. It has been shown that this can be accomplished through a convective flow that is radially inward under the center of the antenna, and swirls around the ends of the FRC and then back towards the midplane on the connected outer field lines.⁶ To better understand this mechanism, consider the θ -component of the generalized Ohm's law, $E_\theta = \eta J_\theta + \nu_r B_z + 1/en \langle J_z B_r \rangle$, where E_θ is the azimuthal electric field, η is the plasma resistivity, J_θ is the azimuthal current, ν_r is the radial inward plasma flow driven by the RMF, B_z is the axial magnetic field, and $\langle J_z B_r \rangle$ is the average of the oscillating $J_z B_r$ with J_z the RMF induced axial current and B_r the radial component of the RMF. J_θ is normally negative and $\langle J_z B_r \rangle$ is normally positive in the region where the RMF has penetrated. Consider the case of radially inward plasma flow at the mid-plane, with the RMF penetrated slightly beyond the null. Then in the region outside the null, the 1st, and 2nd terms on the right-hand side

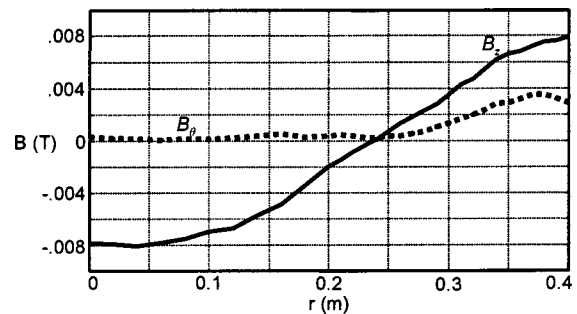


FIG. 3. Experimentally measured magnetic profiles where the RMF, at the applied frequency, did not penetrate to the magnetic field null.

(RHS) are negative, while the 3rd term is positive. In the inner region where the 3rd term is near zero, the first term is still negative, but the second term is positive. Thus with the appropriate flow, an equilibrium can be reached with E_θ zero everywhere. This has been demonstrated numerically,⁶ and is thought to explain the experimental results.^{4,5} It should be noted that at the magnetic field null B_z is zero, so in equilibrium the RMF must penetrate beyond the null for the $\langle J_z B_r \rangle$ term to balance the ηJ_θ term there.

III. EDGE DRIVEN MODE

Recently the TCS experiment was modified by wrapping flux conserving straps around the quartz tube at a radius of $r_c = 0.41$ m, thus making the effective coil radius much closer to the wall radius $r_w = 0.40$ m. The intent of the straps was to help prevent the FRC's separatrix from making wall contact. Although this modification did not increase the effectiveness of the RMF current drive, it did make the experiment much more reproducible on a shot-to-shot basis. However, with this change, a significantly different magnetic profile was often observed. The RMF was confined to a region near the radial edge of the FRC, and did not penetrate to the magnetic null; an absolute requirement for equilibrium according to the argument of the previous section. For this reason, we refer to this mode of current drive as "edge-driven mode."

Figure 3 shows a typical magnetic field profile for a shot where the RMF did not penetrate to the magnetic field null. Notice how the axial magnetic field increases linearly with no tendency to be steeper in the outer edge where the RMF is applying a torque, and little tendency to flatten near the null, unlike the traces shown in Fig. 1. Other parameters of interest at the time of this radial profile were: $f_{\text{RMF}} = 236$ kHz, $T_{\text{total}} = 22$ eV, density at the field null $n_0 = 8 \times 10^{18} \text{ m}^{-3}$, separatrix radius $r_s = 0.35$ m, and $\zeta = 0.13$. It should be noted that edge-driven mode was typical for these high RMF frequency, low ζ shots.

It was found that when the numerical model was run with a resistivity profile that was sharply peaked near the vacuum vessel wall, magnetic profiles similar to the edge-driven experimental observations were predicted. This phenomenon was initially found when the Chodura resistivity⁹ formula was added to the code, expressed as:

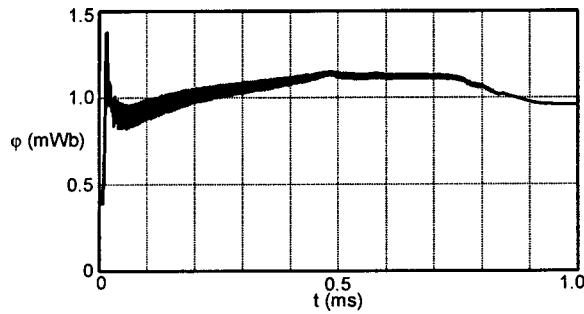


FIG. 4. Time history of trapped flux from a simulation with a resistivity profile that peaked near the vacuum vessel wall.

$$\eta_{\text{chod}} = \frac{m_e v_{\text{chod}}}{n e^2},$$

where

$$v_{\text{chod}} = C_c \omega_{pi} (1 - e^{-|v_e/fv_s|}).$$

C_c and f are input parameters with magnitudes in the vicinity of 0.01 and 3.0, respectively, n is the plasma density, v_e is the electron drift velocity relative to the ions, v_s is the sound velocity, and ω_{pi} is the ion plasma frequency. These parameters lead to a resistivity that varies approximately as $\eta \propto v_e/v_s \sqrt{n}$, which tend to be peaked near the wall for an RMF driven plasma. However, this resistivity varies strongly in both space and time and made the interpretation of numerical results somewhat difficult. For the calculations reported in this paper, a simple time independent resistivity profile given by

$$\eta = \eta_0 + \eta_{\text{edge}} (1 + \exp((r_0 - r)/\chi))^{-1},$$

was used, with parameters $\eta_0 = 31 \mu\Omega \text{ m}$, $\eta_{\text{edge}} = 1200 \mu\Omega \text{ m}$, $r_0 = 0.35 \text{ m}$, and $\chi = 0.01 \text{ m}$ assumed for the perpendicular resistivity. The parameter values for the parallel resistivity were the same, except for the parameter η_0 (only affects central region) which was half as large.

The code was initialized with an FRC profile, but no RMF. A 235.5 kHz RMF that began, at $t=0$, to quickly ramp up to a vacuum value of 2.5 mT, was applied as a boundary condition. The temperature was clamped at a maximum value of 30 eV, and the ions were allowed to spin up to a frequency of 4.5 kHz, on the order of typical experimental values. The time history of the trapped flux ϕ for this calculation is shown in Fig. 4. After about 20 μs , the RMF had penetrated deeply into the FRC, driving the trapped flux up to about 1.4 mWb. The FRC responded to this increased flux by growing radially, increasing the external field, and consequently the density, since the temperature was clamped at 30 eV. The RMF was unable to sustain the current for these conditions and the inner penetrated field lines tore off, leaving an inner *structure* that rotated more slowly than the RMF. After this, the trapped flux grew slowly for about 0.5 ms, where it came to a quasi-equilibrium value until about 0.75 ms. As can be seen in the figure, the magnitude of the trapped flux had a high frequency oscillation during this period.

Figure 5 shows a typical magnetic field profile during

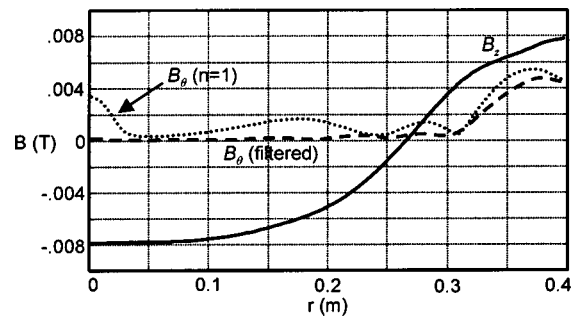


FIG. 5. Magnetic field profile from a simulation with a resistivity profile that peaks near the vacuum vessel wall.

the quasi-equilibrium period. Note that there are two curves for the B_θ profile. The curve labeled “ $n=1$ ” is the magnitude of the $n=1$ component of B_θ in the code, while the “filtered” curve is a value that would be plotted if it were measured by an internal probe and processed using the same methodology that is used in the experiment, where B_θ was measured as a function of time and then passed through a notch filter at $\pm 10 \text{ kHz}$ either side of f_{RMF} . The envelope of this signal is then calculated and plotted as a function of r at the specified time. In the inner region, this curve has a much lower value than the dotted curve because the slower rotation of the inner structure shifts the frequency of the $n=1$ component outside the range of the notch filter. The data for the B_z curve were passed through a 10 kHz low-pass filter so that it also represents an averaged profile.

When Fig. 5 is compared with the experimental data of Fig. 3, we note some striking similarities. First the RMF (especially as seen in the filtered curve) drops to a very low value well before the magnetic field null. Second, the B_z profile now has no tendency to flatten near the field null. Thus, this simulation appears to be in much better agreement with the experimental data than previous calculations where a constant uniform resistivity was used. The next few paragraphs will explore the current-drive mechanism that is active in the simulation during the period when the RMF does not penetrate to the null. Then more data will be presented to show that the same physical mechanism appears to be active in the experiment.

While the RMF amplitude appears to be small at the null, there is still a significant B_r and J_z there, but rotating at a frequency significantly slower than the RMF. This is important because $\langle J_z B_r \rangle$ is the only term in the generalized Ohm’s law that can balance ηJ_θ there. The slowly rotating magnetic structure that has formed in the inner portion of the FRC is applying a torque to the electrons there. But to do so, a torque must also be transferred to the magnetic structure from the outer RMF.

Figure 6 shows a sequence of magnetic field line plots as the applied RMF makes a full rotation relative to the inner structure. This figure is plotted in a frame of reference that rotates with the RMF so that the applied RMF always appears vertical, and thus the inner structure appears to rotate in a clockwise direction. In fact, both the RMF and the inner field-lines rotate in a counter-clockwise direction, but the inner field lines rotate at a much slower rate. By examining

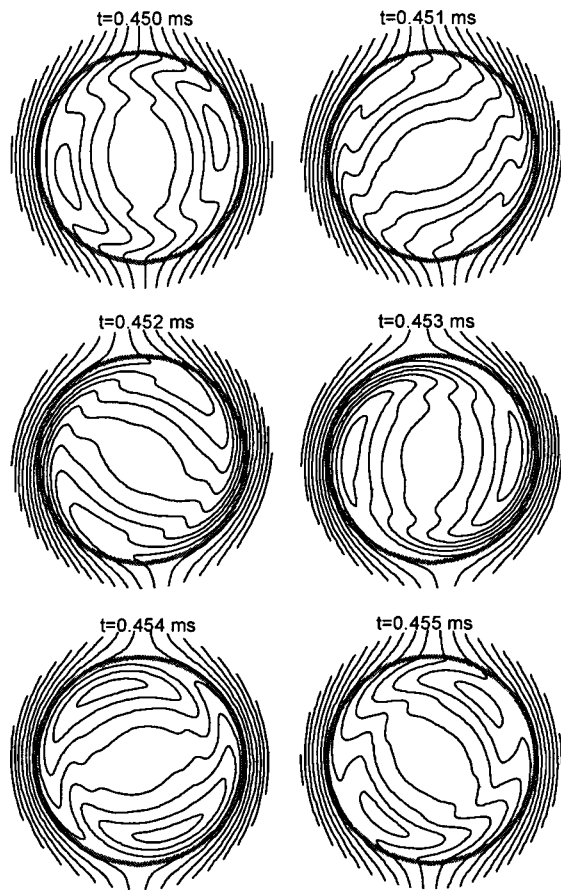


FIG. 6. Time sequence of the calculated RMF field lines as the primary RMF makes a full rotation relative to the inner structure. The circle indicates the position of the vacuum-plasma boundary.

this sequence of field-line plots, it is found that the magnetic field lines tear and then reconnect each time the RMF makes a full rotation relative to the inner field-lines. When the field lines first-reconnect they are bent so that a retarding torque is applied to the inner structure. As the outer RMF rotates further, more field-lines reconnect and a larger positive torque is applied ($t=0.452$ ms). Thus a net oscillating torque is applied to the inner structure and consequently the electrons. The total magnetic field contains a large component in the z direction, so the field lines shown in Fig. 6 should be thought of as a projection of the total field onto the $r-\theta$ plane. In a real finite-length FRC the total field geometry would be more complex, but it is still expected that the magnetic field lines would tear and reconnect each time the RMF makes a full rotation relative to the more slowly rotating inner field-lines.

The frequency of the oscillating torque is $f_{\text{RMF}} \cdot f_{\text{struct}}$ where f_{struct} is the rotation frequency of the inner structure. The oscillating torque applied to the electrons causes the oscillations in the trapped flux ϕ_o , shown in Fig. 4. Similar oscillations can also be seen in the external axial magnetic field, $B_{z\text{Ext}}$. It will now be shown with a spectral analysis, that this oscillation frequency is $f_{\text{RMF}} \cdot f_{\text{struct}}$, and that exactly the same oscillations appear in the experimental data.

Figure 7 shows the spectral amplitude of the external B_z and the internal B_θ at a specific radial location and in a time window of 0.5 to 0.75 ms (a period of quasi-equilibrium). As

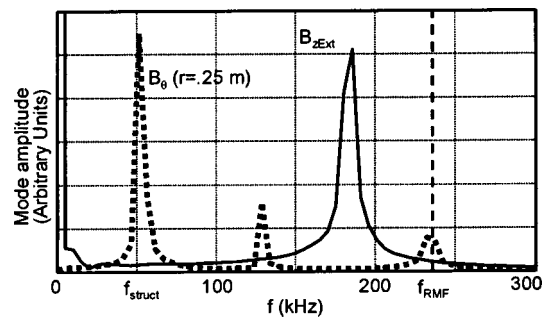


FIG. 7. Spectral amplitude of the calculated external $B_{z\text{Ext}}$ (solid line) and internal B_θ (dotted line) during the time window of 0.5–0.7 ms.

expected, the internal B_θ has a strong spike at the rotation frequency of the inner structure, and $B_{z\text{Ext}}$ has a strong spike at $f_{\text{RMF}} \cdot f_{\text{struct}}$. Figure 8 shows the same plot, but for an experimental shot with identical conditions to that shown in Fig. 3, except the internal probe was rotated to measure only B_θ . The spectral analysis is done in the time window of 0.8–1.3 ms, a period of quasi-equilibrium. Like the numerical data, Fig. 8 shows a distinct spike at a low frequency labeled f_{struct} that is being interpreted as the rotation frequency of an inner structure, as well as a strong spike in $B_{z\text{Ext}}$ at a frequency of $f_{\text{RMF}} \cdot f_{\text{struct}}$. A loop external to the vacuum vessel and internal to the flux coils, that azimuthally averaged the axial magnetic field B_z , was used to measure $B_{z\text{Ext}}$. This signal also had a spectral spike at f_{RMF} , due to noise pickup from the RMF in which it is immersed.

It is also informative to look at a contour map of B_θ as a function of time and radius inside the plasma, as shown in Figs. 9 and 10 for the numerical and experimental data, respectively. The experimental data were taken from the same shot as Fig. 8, where the probe was rotated to measure B_θ only, so the full bandwidth can be displayed. The oscillating bands at the top edge of these plots are separated by one RMF period. The bands drift to the right as they move in radially due to the phase shift that occurs as the electrons drag the field lines in the clockwise direction. In the calculation (Fig. 9) there is a distinct break around $r=0.3$ m where the field lines tear and the slower rotating internal structure begins. The experimental data are more complex but the lower frequency component, indicating a slowly rotating structure, is clearly visible. However, a significant fraction of the low amplitude signal in the inner region is at

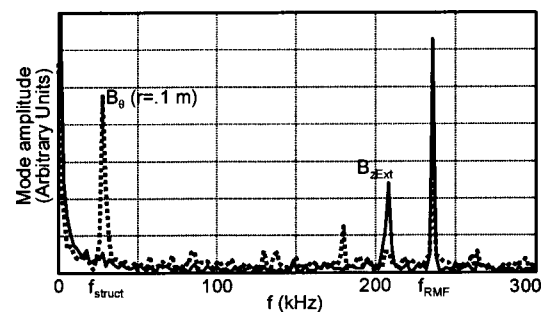


FIG. 8. Spectral amplitude of the measured external $B_{z\text{Ext}}$ (solid line) and internal B_θ (dotted line) during the time window of 0.8–1.3 ms.

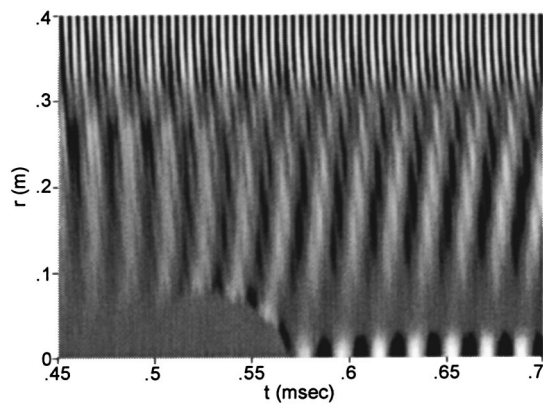


FIG. 9. B_θ contour maps as a function of radius and time from the numerical simulation.

the RMF frequency. The experimental data show the inner structure rotating at a significantly lower frequency than the numerical data, reflecting a lower value for the parameter ζ (about 0.13 for the experiment vs about 0.20 for the calculation).

IV. DISCUSSION AND CONCLUSIONS

A new mode of RMF current drive, which we are calling edge-driven mode, has been identified. In this mode, the primary RMF is confined to the edge of the FRC, and its torque is transferred to a magnetic structure that co-rotates with the inner electrons through a tearing and reconnection process near the edge of the FRC. The inner structure rotates at a frequency downshifted by a factor of approximately ξ from the frequency of the RMF applied at the edge. This phenomenon occurs in numerical simulations when a resistivity profile that is sharply peaked near the plasma edge is used, suggesting that the experimental plasma may also have a resistivity that is peaked near the vacuum boundary, and much smaller in the core of the FRC. This profile could be produced by micro-instabilities since the RMF induces large electron velocities at large radius, or due to other effects introduced by the RMF itself.⁷ The physical mechanism has

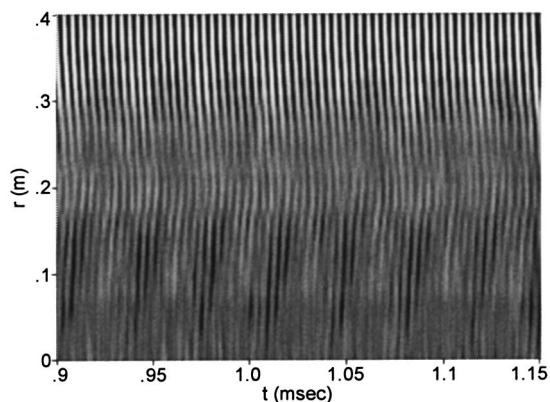


FIG. 10. B_θ contour maps as a function of radius and time as measured by the internal probe.

a unique *fingerprint* where the external magnetic field $B_{z\text{Ext}}$ has a fluctuation at the RMF frequency downshifted by the rotation frequency of the inner structure. This *fingerprint* is clearly evident in the experimental data.

With this mode of RMF current-drive, there are two distinct regions in the plasma. In the outer region, the primary RMF penetrates and rotates with frequency f_{RMF} , while in the inner region a rotating magnetic structure forms and rotates with a frequency of f_{struct} . Torque is transferred from the outer primary RMF to the inner structure through a tearing and reconnection process that takes place at a frequency of $f_{\text{RMF}} - f_{\text{struct}}$. The plasma in the inner region experiences RMF current drive, but at the downshifted frequency, f_{struct} . It is expected that the condition $f_{\text{struct}} \gg f_{\text{ci}}$, where $f_{\text{ci}} = eB_{\text{struct}}/2\pi m_i$, should be obeyed. For the numerical (experimental) data we find $f_{\text{struct}} = 51$ (28) kHz, $B_{\text{struct}} = 0.001$ (0.0004) T, and $f_{\text{ci}} = 7.6$ (3) kHz, thus the condition $f_{\text{struct}} \gg f_{\text{ci}}$ is clearly satisfied. Likewise, we expect that the parameter $\gamma = \omega_{\text{ce}}/\nu_\perp$ should be of at least the same magnitude as the parameter $\lambda = r_s/\delta$, where $\delta = (2\eta/\mu_o\omega_{\text{RMF}})^{1/2}$ is the skin depth, ω_{ce} is the plasma electron cyclotron frequency in the RMF, ν_\perp is the electron-ion collision frequency, and ω_{RMF} is $2\pi f_{\text{RMF}}$. For the numerical calculation we find $\gamma = 31.5$, and $\lambda = 28$ in the inner region. The resistivity of the inner region was not known in the experiment, so the experimental values of these parameters cannot be calculated at this time.

In the experiment an average resistivity was estimated by doing a power balance between the power input to the antenna and the power absorbed by the plasma, assuming a rigid-rotor profile and uniform resistivity. A similar average can be calculated for the code by using the Poynting vector at the calculation boundary to estimate the input RMF power. Using this simple estimate, both the experimental data and numerical calculation yield an average η_\perp of about $250 \mu\Omega \text{ m}$. As discussed in Sec. III, the actual resistivity used in the calculation was $31 \mu\Omega \text{ m}$ in the center and $1200 \mu\Omega \text{ m}$ in the outer region. Thus the calculation's resistivity profile is consistent with experimental observations, but more detailed measurements would be required to estimate the actual profile.

ACKNOWLEDGMENTS

The authors acknowledge many useful discussions with J. T. Slough, H. Y. Guo, and A. L. Hoffman during the course of this work.

This work was carried out under the support of DOE under Grant No. DE-FG03-96ER54376.

¹H. A. Blevin and P. C. Thonemann, Nucl. Fusion Suppl. **55**, Pt.1 (1962).

²I. R. Jones, Phys. Plasmas **6**, 1950 (1999).

³A. L. Hoffman, H. Y. Guo, J. T. Slough, S. J. Tobin, L. S. Schrank, W. A. Reass, and G. A. Wurden, Fusion Technol. **41**, 92 (2002).

⁴H. Y. Guo, A. L. Hoffman, R. D. Brooks, A. M. Peter, Z. A. Pietrzyk, S. J. Tobin, and G. R. Votroubek, Phys. Plasmas **9**, 185 (2002).

⁵J. T. Slough and K. E. Miller, Phys. Plasmas **7**, 1945 (2000).

⁶R. D. Milroy, Phys. Plasmas **7**, 4135 (2000).

⁷A. L. Hoffman, H. Y. Guo, R. D. Milroy, and Z. A. Pietrzyk, Nucl. Fusion **43**, 1091 (2003).

⁸J. T. Slough and K. E. Miller, Phys. Rev. Lett. **85**, 1444 (2000).

⁹R. Chodura, Nucl. Fusion **15**, 65 (1975).